NASA TECHNICAL NOTE
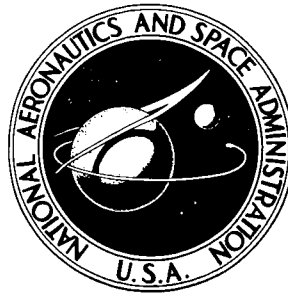
NASA TN D-7448

BALL MOTION AND SLIDING FRICTION IN AN ARCHED OUTER-RACE BALL BEARING

by Bernard J. Hamrock

Lewis Research Center

Cleveland, Ohio 44135

1. Report No. NASA TN D-7448	2. Government Accession No.	3. Recipient's Catalog No.
4. Title and Subtitle BALL MOTION AND SLIDING FRICTION IN AN ARCHED OUTER-RACE BALL BEARING		5. Report Date January 1974
		6. Performing Organization Code
7. Author(s) Bernard J. Hamrock		8. Performing Organization Report No. E-7607
9. Performing Organization Name and Address Lewis Research Center National Aeronautics and Space Administration Cleveland, Ohio 44135		10. Work Unit No. 501-24
		11. Contract or Grant No.
		13. Type of Report and Period Covered Technical Note
12. Sponsoring Agency Name and Address National Aeronautics and Space Administration Washington, D. C. 20546		
		14. Sponsoring Agency Code
15. Supplementary Notes		

16. Abstract

The motion of the ball and sliding friction in an arched outer-race ball bearing under thrust load is analyzed. Fatigue life evaluations were made. The analysis is applied to a 150-millimeter-bore ball bearing. The results indicated that for high-speed light-load applications the arched bearing has significant improvement in fatigue life over that of a conventional hearing. An arching of 0.254 mm (0.01 in.) was found to be optimal. Also, for an arched bearing a considerable amount of spinning occurs at the outer-race contacts.

17. Key Words (Suggested by Author(s)) Ball bearing Arched outer race Dynamic analysis Lubrication Life evaluation	18. Distribution Statement Unclassified - unlimited Cat. 15		
19. Security Classif. (of this report) Unclassified	20. Security Classif. (of this page) Unclassified	21. No. of Pages 45	22. Price* $3.00

BALL MOTION AND SLIDING FRICTION IN AN ARCHED

OUTER-RACE BALL BEARING

by Bernard J. Hamrock

Lewis Research Center

SUMMARY

The motion of the ball and sliding friction in an arched outer-race ball bearing under thrust load is analyzed. This motion of the ball and sliding friction is expressed in terms of the inertial effects on the ball and the frictional resistance resulting from interfacial slip at the contact areas. The solution of seven simultaneous equations involving double integrals for which closed form solution cannot be found is required. Fatigue life evaluations via Lundberg-Palmgren were made. The similar analysis of a conventional bearing can be directly obtained from the arched bearing analysis by simply letting the amount of arching be zero and not considering equations related to the unloaded half of the outer race. The analysis is applied to a 150-millimeter-bore ball bearing.

The results indicated that for high-speed light-load applications the arched outer-race ball bearing has significant improvement in fatigue life over that of a conventional bearing. An arching of 0.254 millimeter (0.01 in.) was found to be an optimal. For an arched bearing it was also found that a considerable amount of spinning occurs at the outer-race contacts.

INTRODUCTION

Aircraft gas turbine engine rotor bearings currently operate in the speed range from 1.5 to 2.0 million DN (bearing bore in mm times shaft speed in rpm). It is estimated that engine designs of the next decade will require bearings to operate at DN values of 3 million or more (ref. 1). In this DN range analyses (refs. 2 and 3) predict a prohibitive reduction in bearing fatigue life due to the high centrifugal forces developed between the rolling elements and the outer race.

An approach to the high-speed bearing problem is an arched outer-race ball bearing. In this bearing, when centrifugal forces become large, the contact load is shared

by two outer-race contacts instead of just one outer-race contact as in conventional ball bearings. A first-order thrust load analysis of an arched outer-race ball bearing that considers centrifugal forces but that neglects gyroscopics, elastohydrodynamics, and sliding friction was performed (refs. 4 and 5). The analysis was applied to a 150-millimeter-bore, angular-contact ball bearing. The results indicated that an arched bearing is highly desirable for high-speed applications. In particular, for a DN value of 3 million (20 000 rpm) and an applied axial load of 4450 newtons (1000 lb), an arched bearing shows an improvement in life of 306 percent over that of a conventional bearing.

The objective of the work described in this report was to conduct fatigue life analysis of the arched outer-race ball bearing while considering the complete motion of the ball as well as the sliding friction. A comparison will be made with a conventional ball bearing as well as comparing the results of references 4 and 5 (where only centrifugal force was considered) with the present analysis where the complete motion of the ball and sliding friction is considered. The analysis will neglect elastohydrodynamics and thermal effects. Furthermore, the approach to be used is similar to that used by Jones (ref. 2) in analyzing a conventional ball bearing.

SYMBOLS

A	distance between raceway groove curvature centers
$\mathscr{A}$	left-side outer-race curvature center
a	semimajor axis of projected contact ellipse
B	$f_o + f_i - 1 = A/D$
$\mathscr{B}$	ball center, initial
b	semiminor axis of projected contact ellipse
$\mathscr{C}$	initial position, inner-raceway groove curvature center
c	inner-race bore
D	ball diameter
$\mathscr{D}$	right-side outer-race curvature center
d	raceway diameter
d_m	pitch diameter, initial
$\bar{d}_m$	pitch diameter after dynamic effects have acted on ball
E	defined by eq. (150)
$\mathscr{E}$	elliptical integral of second kind

$e_1, e_2, \ldots, e_7$	defined by eqs. (123) to (129)
F	force
F_a	axially applied load
$\mathscr{F}$	elliptical integral of first kind
f	r/D
$\mathscr{G}$	inner-race contact, initial
g	amount of arching, or width of material removed from outer race of conventional bearing
$\mathscr{H}$	left outer-race contact, initial
h	distance from top of arch to top of ball when bearing is in radial contact position
I_P	polar moment of inertia of ball
$\mathscr{I}$	inner-race contact, final
J	function of k defined by eq. (33)
$\overline{J}$	Jacobian defined by eq. (136)
$\mathscr{J}$	left outer-race contact, final
K	load-deflection constant
$\mathscr{K}$	right outer-race contact, final
k	a/b
L	life, hr
$\mathscr{L}$	ball center, final
M	frictional moments
$\overline{M}$	inertia moments
$\mathscr{M}$	final position, inner-raceway groove curvature center
m	ball mass
$\mathscr{N}$	tip of arch
n	rotational speed
P	basic dynamic capacity of raceway contact
P_d	bearing diametral clearance
P_e	free end play

Q	ball normal load
q	X/a
R	radius of deformed pressure surface in plane of major axis of pressure ellipse
r	raceway groove curvature radius
$\bar{r}$	$\sqrt{R^2 - X^2} - \sqrt{R^2 - a^2} + \sqrt{\left(\dfrac{D}{2}\right)^2 - a^2}$
r'	effective rolling radius of ball
S_d	bearing diametral play
S_X	axial distance between final position of inner and left outer-raceway groove curvature center
S_Z	radial distance between final position of inner-raceway groove cruvature center and right or left outer-raceway groove curvature center
$s_1, s_2, \ldots, s_8$	initial guesses of V, W, δ_a, α', β', r'_{0l}, and r'_i
T	τ_0/σ_{max}
T_1	$\left(\tau_0/\sigma_{max}\right)_{k=1}$
t	Y/b
U', V', W'	coordinate system defined in report
u	number of stress cycles per revolution
V	radial projection of distance between ball center and outer-raceway groove curvature center
W	axial projection of distance between ball center and outer-raceway groove curvature center
X, Y, Z	coordinate system defined in report
x, y, z	coordinate system defined in report
x', y', z'	coordinate system defined in report
Z	number of balls
α	radical contact angle
$\alpha'\beta'$	angles defining direction of ω_B

4

β	axial contact angle, initial
Γ	curvature difference
γ	$D \cos \beta / \overline{d_m}$
Δ	distance between raceway groove curvature and final position of ball center
δ	contact deformation
δ_a	axial displacement
δ^*	defined by eq. (39)
ζ	ratio of depth of maximum shear stress to semiminor axis
ζ_1	$(\zeta)_{k=1}$
η	defined by eq. (10)
θ	defined by eq. (113)
Λ	density
λ	modulus of elasticity
μ	coefficient of friction
ξ	Poisson's ratio
ρ	curvature sum
σ_{max}	maximum normal stress
τ_o	maximum orthogonal subsurface shear stress
Υ	$\sqrt{x^2 + Y^2}$
φ	auxiliary angle
ψ	defined by eq. (114)
Ω	absolute angular velocity
Ω_c	orbital angular velocity of balls about bearing axis
ω	relative angular velocity
ω_B	angular velocity of ball about its center

Subscripts:

i	inner race
o	outer race

o l	outer left
or	outer right
R	rolling
S	spinning
X, Y, Z	coordinate system defined in report
x', y', z'	coordinate system defined in report

ARCHED-BEARING GEOMETRY

Figure 1 shows how the arched outer race is made. A conventional outer race is shown in figure 1(a) with a race radius of r_o. Also shown in figure 1(a) is the portion of the conventional outer race that is removed in forming an arched outer race. Figure 1(b) shows the arched outer race with the portion of length g removed. Note that there are now two outer-race radius centers separated by a distance g. With modern technology being what it is, an arched outer race can be machined in one piece.

Figure 2 shows the arched bearing while in a noncontacting position. Here the pitch diameter d_m, diametral clearance P_d, diametral play S_d, and raceway diameters d_i and d_o are defined. The diametral play is the total amount of radial movement allowed in the bearing. Furthermore, the diametral clearance is the diametral play plus two times the distance from the bottom of the ball to the tip of the arch when the bearing is in a radial contact position.

Figure 3 shows the arched bearing in a radial contact position. Instead of contacting at one point at the bottom of the outer raceway, the ball contacts at two points separated by an angle 2α. From figure 3 the radial contact angle α can be written as

$$\alpha = \sin^{-1}\left(\frac{g}{2r_o - D}\right) \tag{1}$$

A distance that needs to be formulated is the distance from the tip of the arch to the bottom of the ball when the ball and raceway are in the radial contact position (as shown in fig. 3). This distance is defined as h. From figure 3(b) and the Pythagorian theorem and solving for h the following equation can be written:

$$h = -\frac{D}{2} - \left(r_o - \frac{D}{2}\right)\cos\alpha + \frac{1}{2}\left[D(4r_o - D) + \left(2r_o - D\right)^2 \cos^2\alpha\right]^{1/2} \tag{2}$$

Note that, as one might expect, as $\alpha \rightarrow 0^O$, $h \rightarrow 0$. With h known, a number of conventional bearing parameters can be formulated from figures 2 and 3. The outer-raceway diameter may be written as

$$d_o = \bar{d}_i + P_d + 2D \tag{3}$$

where

$$P_d = S_d + 2h \tag{4}$$

In equation (3) $\bar{d}_i$ is the inner-raceway diameter after centrifugal growth has been considered. Using the centrifugal growth equation found in Timoshenko (ref. 6) the inner-raceway diameter will expand according to the following formulation:

$$\bar{d}_i = d_i + \frac{\Lambda d_i}{1544 \lambda_i} \left(\frac{n_i \pi}{30} \right)^2 \left[\left(\frac{d_i}{2} \right)^2 (1 - \xi_i) + \left(\frac{c}{2} \right)^2 (3 + \xi_i) \right] \tag{5}$$

From equations (3) and (4) the diametral play can be written as

$$S_d = d_o - \bar{d}_i - 2D - 2h \tag{6}$$

The pitch diameter d_m from figure 2 can be expressed as

$$d_m = \bar{d}_i + \frac{S_d}{2} + D \tag{7}$$

Figure 4 shows the arched bearing while in the axial position. From this figure the distance between the center of curvature of the inner and left outer-race can be written as

$$A = r_o + r_i - D$$

With $f_o = r_o D$ and $f_i = r_i D$ this equation becomes

$$A = BD \tag{8}$$

where

$$B = f_o + f_i - 1 \tag{9}$$

From figure 4(b) the following equation can be written

$$\eta = r_o - \sqrt{r_o^2 - \left(\frac{g}{2}\right)^2} \tag{10}$$

With η known the contact angle can be expressed as

$$\beta = \cos^{-1}\left(\frac{A - \dfrac{P_d}{2} - \eta}{A}\right) \tag{11}$$

The end play of an arched bearing is

$$P_e = 2A \sin \beta - g \tag{12}$$

CONTACT GEOMETRY

From the experimental work of Haines and Edmonds (ref. 7), it is observed that the arched bearing will initially operate with two-point contact at the lower speeds and then with three-point contact at higher speeds when the centrifugal forces become significant. When centrifugal force acts on the ball, the inner- and outer-raceway contact angles are dissimilar; therefore, the lines of action between raceway groove curvature radius centers become discontinuous (see fig. 5). In figure 5 the left and right outer-raceway groove curvature centers $\mathcal{A}$ and $\mathcal{B}$ are fixed in space, and the inner-raceway groove curvature center $\mathcal{C}$ moves axially relative to those fixed centers. The initial portion of the analysis (given in ref. 5) is repeated here for the convenience of the reader.

Figure 5 gives the distance between the fixed right and left outer-raceway groove curvature centers $\mathcal{A}$ or $\mathcal{B}$ and the final position of the ball center $\mathcal{L}$ as:

$$\Delta_{ol} = r_o - \frac{D}{2} + \delta_{ol} = (f_o - 0.5)D + \delta_{ol} \tag{13}$$

$$\Delta_{or} = (f_o - 0.5)D + \delta_{or} \tag{14}$$

8

where $\delta_{o l}$ is the normal contact deformation at the left outer-raceway center and δ_{or} is the normal contact deformation of the right outer-raceway center. Similarly, the distance between the final inner-raceway groove curvature center $\mathscr{M}$ and the final position of the ball center $\mathscr{L}$ is

$$\Delta_i = (f_i - 0.5)D + \delta_i \tag{15}$$

where δ_i is the normal contact deformation at the inner-raceway center.

The axial distance between the final position of the inner and left outer-raceway groove curvature center is

$$S_X = A \sin \beta + \delta_a \tag{16}$$

where δ_a is the axial displacement. The radial distance between the final position of the inner-raceway groove curvature center and the right or left outer-raceway groove curvature center is

$$S_Z = A \cos \beta \tag{17}$$

From figure 5 and equations (13) to (17) the following equations can be written:

$$\beta_{or} = \sin^{-1}\left[\frac{g - W}{(f_o - 0.5)D + \delta_{or}}\right] \tag{18}$$

$$\beta_{o l} = \sin^{-1}\left[\frac{W}{(f_o - 0.5)D + \delta_{o l}}\right] \tag{19}$$

$$\beta_i = \sin^{-1}\left[\frac{A \sin \beta + \delta_o - W}{(f_i - 0.5)D + \delta_i}\right] \tag{20}$$

Using the Pythagorean theorem and regrouping terms results in

$$\delta_{or} = \sqrt{V^2 + (g - W)^2} - D(f_o - 0.5) \tag{21}$$

$$\delta_{o l} = \sqrt{V^2 + W^2} - D(f_o - 0.5) \tag{22}$$

$$\delta_i = \sqrt{(A \cos \beta - V)^2 + (A \sin \beta + \delta_o - W)^2} - D(f_i - 0.5) \tag{23}$$

The normal loads are related to the normal contact deformation in the following way:

$$Q = K \delta^{1.5} \tag{24}$$

With the proper subscripting of i, $o\ell$, and or this equation could represent the normal loads of the inner ring Q_i, the left outer ring $Q_{o\ell}$, or the right outer ring Q_{or}. Having defined the normal load in terms of the load deflection constant, one needs next to develop the equations for the load deflection constants.

LOAD-DEFLECTION CONSTANTS

Figure 6 shows the position of the ball and raceway groove curvature centers and contacts with and without dynamic effects acting on the ball. In this figure the unbarred values represent initial locations, and the barred values represent final locations when dynamic effects have acted on the ball. From this figure the pitch diameter when dynamic effects have acted on the ball is

$$\overline{d}_m = d_m + 2\left[(f_o - 0.5)D + \delta_{o\ell}\right] \cos \beta_{o\ell} - 2(f_o - 0.5)D \cos \beta \tag{25}$$

The equations for the curvature sum and differences are (from ref. 8)

$$\rho_i = \frac{1}{D}\left(4 - \frac{1}{f_i} + \frac{2\gamma_i}{1 - \gamma_i}\right) \tag{26}$$

$$\rho_{o\ell} = \frac{1}{D}\left(4 - \frac{1}{f_o} - \frac{2\gamma_{o\ell}}{1 + \gamma_{o\ell}}\right) \tag{27}$$

$$\rho_{or} = \frac{1}{D}\left(4 - \frac{1}{f_o} - \frac{2\gamma_{or}}{1 + \gamma_{or}}\right) \tag{28}$$

10

$$\Gamma_i = \frac{\dfrac{1}{f_i} + \dfrac{2\gamma_i}{1 - \gamma_i}}{4 - \dfrac{1}{f_i} + \dfrac{2\gamma_i}{1 - \gamma_i}} \tag{29}$$

$$\Gamma_{ol} = \frac{\dfrac{1}{f_o} - \dfrac{2\gamma_{ol}}{1 + \gamma_{ol}}}{4 - \dfrac{1}{f_o} - \dfrac{2\gamma_{ol}}{1 + \gamma_{ol}}} \tag{30}$$

$$\Gamma_{or} = \frac{\dfrac{1}{f_o} - \dfrac{2\gamma_{or}}{1 + \gamma_{or}}}{4 - \dfrac{1}{f_o} - \dfrac{2\gamma_{or}}{1 + \gamma_{or}}} \tag{31}$$

where

$$\gamma = \frac{D \cos \beta}{d_m} \tag{32}$$

From reference 8 auxiliary equations (33) to (35), relating the curvature difference and the elliptic integrals of the first and second kind, can be written as

$$k = \sqrt{\frac{2\mathscr{F} \cdot \mathscr{E}(1 + \Gamma)}{\mathscr{E}(1 - \Gamma)}} = J(k) \tag{33}$$

$$\mathscr{F} = \int_0^{\pi/2} \left[1 - \left(1 - \frac{1}{k^2}\right)\sin^2 \varphi\right]^{-1/2} d\varphi \tag{34}$$

$$\mathscr{E} = \int_0^{\pi/2} \left[1 - \left(1 - \frac{1}{k^2}\right)\sin^2 \varphi\right]^{1/2} d\varphi \tag{35}$$

11

where

$$k = \frac{a}{b} \tag{36}$$

and where a and b are the semimajor and semiminor axes, respectively, of the projected elliptical area of contact. A one-point iteration method will be used in evaluation equation (33), where

$$k_{n+1} = J(k_n) \tag{37}$$

From reference 8 the load deflection constant can be written as

$$K = \frac{(2)^{5/2}(\delta^*)^{-3/2}(\rho)^{-1/2}}{3\left(\dfrac{1 - \xi_B^2}{\lambda_B} + \dfrac{1 - \xi^2}{\lambda}\right)} \tag{38}$$

where

$$\delta^* = \frac{2\mathscr{F}}{\pi}\left(\frac{\pi}{2k^2 \mathscr{E}}\right)^{1/3} \tag{39}$$

The expressions for the semimajor and semiminor axes, respectively, are:

$$a = \left\{\frac{3k^2 \mathscr{E} Q}{\pi\rho}\left[\frac{\left(1 - \xi_B^2\right)}{\lambda_B} + \frac{\left(1 - \xi^2\right)}{\lambda}\right]\right\}^{1/3} \tag{40}$$

$$b = \frac{a}{k} \tag{41}$$

With proper subscripting of i, ol, and or in equations (38) to (41) three sets of corresponding equations can be obtained corresponding to the inner race and the left and right outer races.

One design constraint is that the left and right outer-race contacts NOT to overlap.

12

The following inequality must be satisfied in order to prevent overlapping of the left and right outer-race contacts:

$$a_{ol} \cos \beta_{ol} + a_{or} \cos \beta_{or} < \frac{D}{2}(\sin \beta_{ol} + \sin \beta_{or}) \qquad (A)$$

If this inequality is not satisfied, then by increasing the amount of arching one can get the inequality to be satisfied.

INERTIA FORCES AND MOMENTS ON BALL

As was mentioned in the introduction, the analysis that follows is that of Jones (ref. 2) with the exception that Jones analyzed a conventional bearing and in this report an arched outer-race ball bearing is analyzed.

Figure 7 shows the instantaneous position of an element of ball mass of a high speed, angular contact bearing. From Jones (ref. 2) the equations for the inertia forces and moments on the ball can be written as

$$F_{x'} = 0 \qquad (42)$$

$$F_{y'} = 0 \qquad (43)$$

$$F_{z'} = m\left(\frac{\overline{d}_m}{2}\right)\Omega_c^2 \qquad (44)$$

$$\overline{M}_{x'} = 0 \qquad (45)$$

$$\overline{M}_{y'} = I_p \omega_B \Omega_c \sin \alpha' \qquad (46)$$

$$\overline{M}_{z'} = -I_p \omega_B \Omega_c \cos \alpha' \sin \beta' \qquad (47)$$

where ω_B is the angular velocity of the ball about its center (θ in ref. 2), Ω_c is the angular velocity of balls about the bearing axis (φ in ref. 2), m is the mass of the ball, and I_p is the polar moment of the inertia of the ball.

RELATIVE MOTIONS OF ROLLING ELEMENTS

Left Outer-Race Contact

Figure 8 shows the contact of the ball with the left outer race. Assume that the ball center is fixed in the plane of the paper. Let the outer race rotate with angular velocity ω_o. The components of the ball rotational angular velocity, which lie in the plane of the paper, are $\omega_{x'}$ and $\omega_{z'}$.

According to Hertz, the radius of the deformed pressure surface in the plane of the major axis of the pressure ellipse for the left outer-race contact is

$$R_{ol} = \frac{2f_o D}{2f_o + 1} = R_{or} = R_o \tag{48}$$

From figure 8, due to the $\omega_o \cos \beta_{ol}$ component, a point (X_{ol}, Y_{ol}) on the left outer race has the linear velocity V'_{1ol} or

$$V'_{1ol} = -\omega_o \cos \beta_{ol} \left[\frac{\overline{d}_m}{2 \cos \beta_{ol}} + \sqrt{R_o^2 - X_{ol}^2} - \sqrt{R_o^2 - a_{ol}^2} + \sqrt{\left(\frac{D}{2}\right)^2 - a_{ol}^2} \right]$$

or

$$V'_{1ol} = -\frac{\overline{d}_m \omega_o}{2} - \overline{r}_{ol} \omega_o \cos \beta_{ol} \tag{49}$$

where

$$\overline{r}_{ol} = \sqrt{R_o^2 - X_{ol}^2} - \sqrt{R_o^2 - a_{ol}^2} + \sqrt{\left(\frac{D}{2}\right)^2 - a_{ol}^2} \tag{50}$$

Because of $\omega_{x'} \cos \beta_{ol}$ and $\omega_{z'} \sin \beta_{ol}$, a point (X_{ol}, Y_{ol}) on the ball has the linear velocity V'_{2ol}, where

$$V'_{2ol} = -\overline{r}_{ol} (\omega_{z'} \sin \beta_{ol} + \omega_{x'} \cos \beta_{ol}) \tag{51}$$

14

The velocity with which the outer race slips on the ball in the Y-direction is

$$V'_{Yol} = V'_{1ol} - V'_{2ol}$$

or

$$V'_{Yol} = -\frac{\bar{d}_m \omega_o}{2} + \bar{r}_{ol}(\omega_{z'} \sin \beta_{ol} + \omega_{x'} \cos \beta_{ol} - \omega_o \cos \beta_{ol}) \tag{52}$$

Because of $\omega_{y'}$ all points within the pressure area have a velocity of slip of race on the ball of V'_{Xol} in the direction of the x'-z' plane and V'_{Xol} is taken as

$$V'_{Xol} = -\omega_{y'} \bar{r}_{ol} \tag{53}$$

Because of the components of velocity, which lie along the line defined by β_{ol}, there is a spin of the race ω_{Sol} with respect to the ball. Because of component $\omega_o \sin \beta_{ol}$, the following can be written:

$$\omega_{1ol} = -\omega_o \sin \beta_{ol} \tag{54}$$

Because of the components $\omega_{z'} \cos \beta_{ol}$ and $\omega_{x'} \sin \beta_{ol}$ the following can be written:

$$\omega_{2ol} = \omega_{z'} \cos \beta_{ol} - \omega_{x'} \sin \beta_{ol} \tag{55}$$

Therefore, the spin of the left outer race with respect to the ball can be written as

$$\omega_{Sol} = \omega_{1ol} - \omega_{2ol}$$

or

$$\omega_{Sol} = -\omega_o \sin \beta_{ol} - \omega_{z'} \cos \beta_{ol} + \omega_{x'} \sin \beta_{ol} \tag{56}$$

In a similar approach, making use of figure 8, one finds the angular velocity of roll of the ball on the left outer-race contact to be

$$\omega_{Rol} = \omega_{x'} \cos \beta_{ol} + \omega_{z'} \sin \beta_{ol} - \omega_o \cos \beta_{ol} \tag{57}$$

Figure 9 shows the contact of the ball with the right outer race. Due to $\omega_0 \cos \beta_{or}$ a point (X_{or}, Y_{or}) on the right outer race has the linear velocity V'_{1or} or

$$V'_{1or} = -\frac{\overline{d}_m \omega_0}{2} - \overline{r}_{or} \omega_0 \cos \beta_{or} \tag{58}$$

where

$$\overline{r}_{or} = \sqrt{R_o^2 - X_{or}^2} - \sqrt{R_o^2 - a_{or}^2} + \sqrt{\left(\frac{D}{2}\right)^2 - a_{or}^2} \tag{59}$$

Because of $\omega_{x'} \cos \beta_{or}$ and $\omega_{z'} \sin \beta_{or}$, a point (X_{or}, Y_{or}) on the ball has the linear velocity V'_{2or}, where

$$V'_{2or} = \overline{r}_{or}(\omega_{z'} \sin \beta_{or} - \omega_{x'} \cos \beta_{or}) \tag{60}$$

The velocity with which the right outer race slips on the ball in the Y-direction is

$$V'_{Yor} = V'_{1or} - V'_{2or}$$

or

$$V'_{Yor} = -\frac{\overline{d}_m \omega_0}{2} + \overline{r}_{or}(\omega_{x'} \cos \beta_{or} - \omega_{z'} \sin \beta_{or} - \omega_0 \cos \beta_{or}) \tag{61}$$

Because of $\omega_{y'}$, all points within the pressure area have a velocity of slip of race on the ball of V'_{Xor} in the x'-z' plane:

$$V'_{Xor} = -\omega_{y'} \overline{r}_{or} \tag{62}$$

Because of the components of velocity, which lie along the line defined by β_{or}, there is a spin of the right outer race, ω_{Sor} with respect to the ball. Because of the component $\omega_0 \sin \beta_{or}$, the following can be written:

$$\omega_{1or} = \omega_0 \sin \beta_{or} \tag{63}$$

16

Because of the components $\omega_{x'} \sin \beta_{or}$ and $\omega_{z'} \cos \beta_{or}$ the following can be written:

$$\omega_{2or} = \omega_{x'} \sin \beta_{or} + \omega_{z'} \cos \beta_{or} \tag{64}$$

Therefore, the spin of the right outer race with respect to the ball can be written as

$$\omega_{Sor} = \omega_{1or} - \omega_{2or}$$

$$\omega_{Sor} = \omega_o \sin \beta_{or} - \omega_{x'} \sin \beta_{or} - \omega_{z'} \cos \beta_{or} \tag{65}$$

In a similar approach, while making use of figure 9, one finds the angular velocity of roll of the ball on the right outer-race contact to be

$$\omega_{Ror} = \omega_{x'} \cos \beta_{or} - \omega_{z'} \sin \beta_{or} - \omega_o \cos \beta_{or} \tag{66}$$

Inner-Race Contact

Figure 10 shows the contact of the ball with the inner race. The radius of curvature of the deformed inner-race pressure surface can be written as

$$R_i = \frac{2f_i D}{2f_i + 1} \tag{67}$$

Because of $\omega_i \cos \beta_i$, a point (X_i, Y_i) on the inner race has the linear velocity V'_{1i} or

$$V'_{1i} = -\frac{\overline{d}_m \omega_i}{2} + \overline{r}_i \omega_i \cos \beta_i \tag{68}$$

where

$$\overline{r}_i = \sqrt{R_i^2 - X_i^2} - \sqrt{R_i^2 - a_i^2} + \sqrt{\left(\frac{D}{2}\right)^2 - a_i^2} \tag{69}$$

Because of $\omega_{x'} \cos \beta_i$ and $\omega_{z'} \sin \beta_i$, a point (X_i, Y_i) on the ball has the linear velocity V'_{2i} or

$$V'_{2i} = \overline{r}_i (\omega_{x'} \cos \beta_i + \omega_{z'} \sin \beta_i) \tag{70}$$

The velocity with which the inner race slips on the ball in the Y-direction is

$$V'_{Yi} = V'_{1i} - V'_{2i}$$

or

$$V'_{Yi} = -\frac{\overline{d}_m \omega_i}{2} + \overline{r}_i(-\omega_{x'} \cos \beta_i - \omega_{z'} \sin \beta_i + \omega_i \cos \beta_i) \qquad (71)$$

Because of $\omega_{y'}$, all points within the pressure area have a velocity of slip of the race on the ball of V'_{Xi} in the direction of the x'-z' plane

$$V'_{Xi} = -\omega_{y'} \overline{r}_i \qquad (72)$$

Because of the components of velocity, which lie along the line defined by β_i, there is a spin of the inner race ω_{Si} with respect to the ball. Due to component $\omega_i \sin \beta_i$ the following can be written:

$$\omega_{1i} = \omega_i \sin \beta_i \qquad (73)$$

Because of the components $\omega_{x'} \sin \beta_i$ and $\omega_{z'} \cos \beta_i$,

$$\omega_{2i} = -\omega_{z'} \cos \beta_i + \omega_{x'} \sin \beta_i \qquad (74)$$

Therefore, the spin of the inner race with respect to the ball can be written as

$$\omega_{Si} = \omega_{1i} - \omega_{2i}$$

or

$$\omega_{Si} = \omega_i \sin \beta_i + \omega_{z'} \cos \beta_i - \omega_{x'} \sin \beta_i \qquad (75)$$

In a similar approach, making use of figure 10, one finds the angular velocity of roll of the ball on the inner-race contact to be

$$\omega_{Ri} = -\omega_{x'} \cos \beta_i - \omega_{z'} \sin \beta_i + \omega_i \cos \beta_i \qquad (76)$$

From figure 7 the following equations can be written:

$$\omega_{x'} = \omega_B \cos \alpha' \cos \beta' \tag{77}$$

$$\omega_{y'} = \omega_B \cos \alpha' \sin \beta' \tag{78}$$

$$\omega_{z'} = \omega_B \sin \alpha' \tag{79}$$

Substituting these equations into equations (52), (53), (56), (57), (61), (62), (65), (66), (71), (72), (75), and (76) gives

$$V'_{Yol} = -\frac{\overline{d}_m \omega_o}{2} + \overline{r}_{ol} \omega_o \left(\frac{\omega_B}{\omega_o} \sin \alpha' \sin \beta_{ol} + \frac{\omega_B}{\omega_o} \cos \alpha' \cos \beta' \cos \beta_{ol} - \cos \beta_{ol} \right) \tag{80}$$

$$V'_{Xol} = -\left(\frac{\omega_B}{\omega_o} \right) \overline{r}_{ol} \omega_o \cos \alpha' \sin \beta' \tag{81}$$

$$\omega_{Sol} = \omega_o \left(\frac{\omega_B}{\omega_o} \cos \alpha' \cos \beta' \sin \beta_{ol} - \frac{\omega_B}{\omega_o} \sin \alpha' \cos \beta_{ol} - \sin \beta_{ol} \right) \tag{82}$$

$$\omega_{Rol} = \omega_o \left[-\cos \beta_{ol}' + \frac{\omega_B}{\omega_o} (\cos \alpha' \cos \beta' \cos \beta_{ol} + \sin \alpha' \sin \beta_{ol}) \right] \tag{83}$$

$$V'_{Yor} = -\frac{\overline{d}_m \omega_o}{2} + \overline{r}_{or} \omega_o \left[\frac{\omega_B}{\omega_o} (\cos \alpha' \cos \beta' \cos \beta_{or} - \sin \alpha' \sin \beta_{or}) - \cos \beta_{or} \right] \tag{84}$$

$$V'_{Xor} = -\frac{\omega_B}{\omega_o} \overline{r}_{or} \omega_o \cos \alpha' \sin \beta' \tag{85}$$

$$\omega_{Sor} = \omega_o \left[\sin \beta_{or} - \frac{\omega_B}{\omega_o} (\cos \alpha' \cos \beta' \sin \beta_{or} + \sin \alpha' \cos \beta_{or}) \right] \tag{86}$$

$$\omega_{Ror} = \omega_o \left[-\cos \beta_{or} + \frac{\omega_B}{\omega_o} (\cos \alpha' \cos \beta' \cos \beta_{or} - \sin \alpha' \sin \beta_{or}) \right] \tag{87}$$

$$V'_{Yi} = -\frac{\overline{d}_m \omega_i}{2} + \overline{r}_i \omega_i \left[\cos \beta_i - \frac{\omega_B}{\omega_i} (\cos \alpha' \cos \beta' \cos \beta_i + \sin \alpha' \sin \beta_i) \right] \tag{88}$$

$$V'_{Xi} = -\frac{\omega_B}{\omega_i} \overline{r}_i \omega_i \cos \alpha' \sin \beta' \tag{89}$$

$$\omega_{Si} = \omega_i \left[\sin \beta_i + \frac{\omega_B}{\omega_i} (\sin \alpha' \cos \beta_i - \cos \alpha' \cos \beta' \sin \beta_i) \right] \tag{90}$$

$$\omega_{Ri} = \omega_i \left[\cos \beta_i - \frac{\omega_B}{\omega_i} (\cos \alpha' \cos \beta' \cos \beta_i + \sin \alpha' \sin \beta_i) \right] \tag{91}$$

From figures 8 to 10 there is some radius denoted as r'_{ol}, r'_{or}, and r'_i, respectively, called the effective rolling radius at which pure rolling occurs. These radii are not necessarily restricted to points that lie on the deformed pressure surfaces if gross slip between the ball and races occurs. At these effective rolling radii r'_{ol}, r'_{or}, and r'_i on the ball, the translational velocities of ball and race is the same. Therefore, from figures 8 to 10 the following equations can be written:

$$-\omega_o \cos \beta_{ol} \left(\frac{\overline{d}_m}{2 \cos \beta_{ol}} + r'_{ol} \right) = -r'_{ol} (\omega_{x'} \cos \beta_{ol} + \omega_{z'} \sin \beta_{ol}) \tag{92}$$

$$-\omega_o \cos \beta_{or} \left(\frac{\overline{d}_m}{2 \cos \beta_{or}} + r'_{or} \right) = r'_{or} (\omega_{z'} \sin \beta_{or} - \omega_{x'} \cos \beta_{or}) \tag{93}$$

$$-\omega_i \cos \beta_i \left(\frac{\overline{d}_m}{2 \cos \beta_i} - r'_i \right) = r'_i (\omega_{x'} \cos \beta_i + \omega_{z'} \sin \beta_i) \tag{94}$$

Making use of equations (77) to (79) and rearranging terms result in

20

$$\frac{\omega_B}{\omega_o} = \frac{\dfrac{\overline{d}_m}{2r'_{ol}} + \cos \beta_{ol}}{\cos \alpha' \cos \beta' \cos \beta_{ol} + \sin \alpha' \sin \beta_{ol}} \tag{95}$$

$$\frac{\omega_B}{\omega_o} = \frac{\dfrac{\overline{d}_m}{2r'_{or}} + \cos \beta_{or}}{\cos \alpha' \cos \beta' \cos \beta_{or} - \sin \alpha' \sin \beta_{or}} \tag{96}$$

$$\frac{\omega_B}{\omega_i} = \frac{-\dfrac{\overline{d}_m}{2r'_i} + \cos \beta_i}{\cos \alpha' \cos \beta' \cos \beta_i + \sin \alpha' \sin \beta_i} \tag{97}$$

From equation (96), solving for r'_{or}, the following equation can be written:

$$r'_{or} = \frac{\dfrac{\overline{d}_m}{2}}{\dfrac{\omega_B}{\omega_o}(\cos \alpha' \cos \beta' \cos \beta_{or} - \sin \alpha' \sin \beta_{or}) - \cos \beta_{or}} \tag{98}$$

Making use of equations (95) to (97), equations (80), (84), and (88) can be rewritten as

$$V'_{Yol} = \frac{\overline{d}_m \omega_o (\overline{r}_{ol} - r'_{ol})}{2r'_{ol}} \tag{99}$$

$$V'_{Yor} = \frac{\overline{d}_m \omega_o (\overline{r}_{or} - r'_{or})}{2r'_{or}} \tag{100}$$

$$V'_{Yi} = \frac{\overline{d}_m \omega_i (\overline{r}_i - r'_i)}{2r'_i} \tag{101}$$

If, instead of the ball center being fixed in space, the outer race is fixed, then the ball center must orbit about the center of the fixed coordinate system with an angular speed of $\Omega_c = -\omega_o$. Therefore, the inner race must rotate with an absolute angular

speed of $\Omega_i = \omega_i + \Omega_c$. Using these relations the relative angular speeds ω_o and ω_i can be described in terms of the absolute angular speed of the inner raceway. From equations (95) and (97) the following can be written:

$$\omega_o = \frac{\omega_i \left(-\dfrac{\overline{d}_m}{2r_i'} + \cos \beta_i \right) (\cos \alpha' \cos \beta' \cos \beta_{ol} + \sin \alpha' \sin \beta_{ol})}{\left(\dfrac{\overline{d}_m}{2r_{ol}'} + \cos \beta_{ol} \right) (\cos \alpha' \cos \beta' \cos \beta_i + \sin \alpha' \sin \beta_i)} \tag{102}$$

Therefore, one can write the relative angular velocity in terms of the inner-race absolute angular speed by the following equations:

$$\omega_i = \frac{\Omega_i \dfrac{\omega_B}{\omega_o}}{\dfrac{\omega_B}{\omega_o} - \dfrac{\omega_B}{\omega_i}} \tag{103}$$

$$\omega_o = \frac{\Omega_i \dfrac{\omega_B}{\omega_i}}{\dfrac{\omega_B}{\omega_o} - \dfrac{\omega_B}{\omega_i}} \tag{104}$$

$$\omega_B = \frac{\Omega_i \dfrac{\omega_B}{\omega_o} \dfrac{\omega_B}{\omega_i}}{\dfrac{\omega_B}{\omega_o} - \dfrac{\omega_B}{\omega_i}} \tag{105}$$

Sliding Friction at Pressure Surface

Figure 11 is an enlarged view of the pressure area at any of the race contacts as viewed from outside of the ball.

Because of the spin velocity ω_S and the linear slip velocities V'_Y and V'_X, an element of area dA at coordinates (X, Y) has resultant velocity of slip V of the race on the ball acting at the angle ψ with respect to the X-direction.

From Jones (ref. 2) the equations for the friction forces and moments can be directly written as

$$F_Y = \frac{3Q\mu}{2\pi} \int_{-1}^{1} \int_{-\sqrt{1-q^2}}^{\sqrt{1-q^2}} \sqrt{1 - q^2 - t^2}\, \cos\psi\, dt\, dq \qquad (106)$$

$$F_X = \frac{3Q\mu}{2\pi} \int_{-1}^{1} \int_{-\sqrt{1-q^2}}^{\sqrt{1-q^2}} \sqrt{1 - q^2 - t^2}\, \sin\psi\, dt\, dq \qquad (107)$$

$$M_S = \frac{3Q\mu a}{2\pi} \int_{-1}^{1} \int_{-\sqrt{1-q^2}}^{\sqrt{1-q^2}} \sqrt{1 - q^2 - t^2}\, \sqrt{q^2 + \frac{t^2}{k^2}}\, \cos(\psi - \theta)\, dt\, dq \qquad (108)$$

$$M_{y'} = \frac{3Q\mu}{2\pi} \int_{-1}^{1} \int_{-\sqrt{1-q^2}}^{\sqrt{1-q^2}} \bar{r}\sqrt{1 - q^2 - t^2}\, \sin\psi\, dt\, dq \qquad (109)$$

$$M_R = \frac{3Q\mu}{2\pi} \int_{-1}^{1} \int_{-\sqrt{1-q^2}}^{\sqrt{1-q^2}} \bar{r}\sqrt{1 - q^2 - t^2}\, \cos\psi\, dt\, dq \qquad (110)$$

where

$$q = \frac{X}{a} \qquad (111)$$

$$t = \frac{Y}{b} \qquad (112)$$

$$\theta = \tan^{-1}\left(\frac{t}{kq}\right) \qquad (113)$$

$$\psi = \tan^{-1}\left(\frac{\dfrac{t}{k} - \dfrac{V'_X}{a\omega_S}}{q + \dfrac{V'_Y}{a\omega_S}}\right) \qquad (114)$$

With proper subscripting of i, ol, and or in equations (106) to (114) three sets of corresponding equations can be obtained for the inner-race, the left, and the right outer-race friction forces and moments.

The coefficient of friction μ will be assumed to be 0.065 (ref. 2) for the calculations.

<div align="center">EQUILIBRIUM CONDITIONS</div>

Figure 12 shows the moments acting on the ball. From this figure the following equations can be written:

$$-M_{Ro l}\sin\beta_{o l} + M_{So l}\cos\beta_{o l} + \overline{M}_{z'} + M_{Ri}\sin\beta_i - M_{Si}\cos\beta_i + M_{Ror}\sin\beta_{or}$$

$$+ M_{Sor}\cos\beta_{or} = 0 \qquad (115)$$

$$-M_{Ro l}\cos\beta_{o l} - M_{So l}\sin\beta_{o l} + M_{Ri}\cos\beta_i + M_{Si}\sin\beta_i - M_{Ror}\cos\beta_{or}$$

$$+ M_{Sor}\sin\beta_{or} = 0 \qquad (116)$$

$$\overline{M}_{y'} - M_{y'o l} - M_{y'or} - M_{y'i} = 0 \qquad (117)$$

24

Figure 13 shows the forces acting on the ball. From this figure the following equations can be written:

$$-Q_{ol} \cos \beta_{ol} - F_{Xol} \sin \beta_{ol} - Q_{or} \cos \beta_{or} + F_{Xor} \sin \beta_{or} + F_{z'} + Q_i \cos \beta_i$$

$$+ F_{Xi} \sin \beta_i = 0 \qquad (118)$$

$$Q_{ol} \sin \beta_{ol} - F_{Xol} \cos \beta_{ol} - Q_{or} \sin \beta_{or} - F_{Xor} \cos \beta_{or} - Q_i \sin \beta_i$$

$$+ F_{Xi} \cos \beta_i = 0 \qquad (119)$$

$$F_{Yol} + F_{Yor} + F_{Yi} = 0 \qquad (120)$$

Ball bearings subject to a pure thrust load have the following relation:

$$Q_i \sin \beta_i - F_{Xi} \cos \beta_i - \frac{F_a}{Z} = 0 \qquad (121)$$

Note that, because of equation (121), equation (119) can be rewritten as

$$Q_{ol} \sin \beta_{ol} - F_{Xol} \cos \beta_{ol} - Q_{or} \sin \beta_{or} - F_{Xor} \cos \beta_{or} - \frac{F_a}{Z} = 0 \qquad (122)$$

Therefore, the seven equations that are necessary for the solution of the seven unknowns V, W, δ_a, α', β', r'_{ol}, and r'_i are the following:

$$-M_{Rol} \sin \beta_{ol} + M_{Sol} \cos \beta_{ol} + \overline{M}_{z'} + M_{Ri} \sin \beta_i - M_{Si} \cos \beta_i + M_{Ror} \sin \beta_{or}$$

$$+ M_{Sor} \cos \beta_{or} = e_1 = 0 \qquad (123)$$

$$-M_{Rol} \cos \beta_{ol} - M_{Sol} \sin \beta_{ol} + M_{Ri} \cos \beta_i + M_{Si} \sin \beta_i - M_{Ror} \cos \beta_{or}$$

$$+ M_{Sor} \sin \beta_{or} = e_2 = 0 \qquad (124)$$

$$\overline{M}'_y - M_{y'ol} - M_{y'or} - M_{y'i} = e_3 = 0 \qquad (125)$$

$$-K_{ol} \, \delta_{ol}^{3/2} \cos \beta_{ol} - F_{Xol} \sin \beta_{ol} - K_{or} \, \delta_{or}^{3/2} \cos \beta_{or} + F_{Xor} \sin \beta_{or} + F_{z'}$$

$$+ K_i \, \delta_i^{3/2} \cos \beta_i + F_{Xi} \sin \beta_i = e_4 = 0 \tag{126}$$

$$K_{ol} \, \delta_{ol}^{3/2} \sin \beta_{ol} - F_{Xol} \cos \beta_{ol} - K_{or} \, \delta_{or}^{3/2} \sin \beta_{or} - F_{Xor} \cos \beta_{or} - \frac{F_a}{Z} = e_5 = 0 \tag{127}$$

$$F_{Yol} + F_{Yor} + F_{Yi} = e_6 = 0 \tag{128}$$

$$K_i \, \delta_i^{3/2} \sin \beta_i - F_{Xi} \cos \beta_i - \frac{F_a}{Z} = e_7 = 0 \tag{129}$$

NUMERICAL ITERATION OF SEVEN SIMULTANEOUS NONLINEAR EQUATIONS

The approach to be used is to first obtain good estimates for V, W, and δ_a. This is accomplished by using the arched bearing computer program used to obtain results in references 4 and 5, where only the centrifugal force acting on the balls is considered. In equations (126), (127), and (129) this amounts to neglecting the friction forces. By doing this we should have a good approximation of the true value of V, W, and δ_a, since the friction forces are small in comparison with the applied forces acting on the contacts.

Having good initial estimates for V, W, and δ_a, we must next determine good initial estimates for r'_{ol} and r'_i. These radii are the radii where there is zero translational slip of the race on the ball. From figures 8 and 10 and equations (50) and (69), one obtains an understanding of what is meant by the barred and primed radii. Equations (50) and (69) can be written in general form as

$$\bar{r} = \sqrt{R^2 - a^2 q^2} - \sqrt{R^2 - a^2} + \sqrt{\left(\frac{D}{2}\right)^2 - a^2} \tag{130}$$

The initial values of r' are

$$r' = \bar{r} \Big|_{q=0.3} \tag{131}$$

26

This will assure us that there is some radius such that zero translational slip of the race on the ball occurs.

Having good initial estimates for V, W, δ_a, r'_{ol}, and r'_i and letting $\alpha' = \beta' = 0$, we can now get to the problem of solving equations (123) to (129). The basic approach will be to express these equations in Taylor's theorem in seven dimensions. Considering only the first two terms of the expansion and rearranging terms in matrix notation, one finds that the equations now are seven simultaneous linear equations. By introducing a two-step algorithm, one is then able to describe the iterative solutions of the seven simultaneous linear equations.

THEOREM

Given the real functions $\displaystyle\sum_{j=1,\ldots}^{7} e_j(V, W, \delta_a, \alpha', \beta', r'_{ol}, r'_i)$ such that $\partial e_j/\partial V, \ldots, \partial e_j/\partial r'_i$, $j = 1, \ldots, 7$ exist and are continuous over defined intervals of the seven parameters, then the seventh dimension Taylor expansion, while neglecting third and higher terms, can be written as

$$e_j(S_1, S_2, \ldots, S_7) \approx e_j(s_1, s_2, \ldots, s_7) + \sum_{i=1,\ldots}^{7} \left.\frac{\partial e_j}{\partial S_i}\right|_{S_i=s_i} (S_i - s_i) \qquad j = 1, 2, \ldots, 7 \quad (132)$$

where s_i initial estimates of V, W, δ_a, α', β', r'_{ol}, and r'_i and $S_i = V$, W, δ_a, α', β', r'_{ol}, r'_i for $i = 1, 2, \ldots, 7$, respectively.

Expanding equation (132) gives

$$e_j(S_1, S_2, \ldots, S_7) \approx e_j(s_1, s_2, \ldots, s_7) + \left.\frac{\partial e_j}{\partial s_1}\right|_{S_i=s_i} (S_1 - s_1)$$

$$+ \left.\frac{\partial e_j}{\partial S_2}\right|_{S_i=s_i} (S_2 - s_2) + \ldots + \left.\frac{\partial e_j}{\partial S_7}\right|_{S_i=s_i} (S_7 - s_7) \qquad j = 1, 2, \ldots, 7 \quad (133)$$

Now in equation (133) we wish to find $(S_1, S_2, \ldots, S_7)$ such that the left side becomes zeros. Therefore, we are led to

$$0 \approx e_j(s_1, s_2, \ldots, s_7) + \left.\frac{\partial e_j}{\partial S_1}\right|_{S_i = s_i} (S_1 - s_1) + \left.\frac{\partial e_j}{\partial S_2}\right|_{S_i = s_i} (S_2 - s_2)$$

$$+ \ldots + \left.\frac{\partial e_j}{\partial S_7}\right|_{S_i = s_i} (S_7 - s_7) \qquad j = 1, 2, \ldots, 7 \quad (134)$$

If the approximation that only the first two terms in the Taylor's expansion is valid, then our system of equations goes from being nonlinear to linear, and, using matrix notation, the linear system can be written as

$$\begin{bmatrix} 0 \\ 0 \\ \cdot \\ \cdot \\ \cdot \\ 0 \end{bmatrix} = \begin{bmatrix} e_1(s_1, s_2, \ldots, s_7) \\ e_2(s_1, s_2, \ldots, s_7) \\ \cdot \\ \cdot \\ \cdot \\ e_7(s_1, s_2, \ldots, s_7) \end{bmatrix} + \overline{J}(S_1, S_2, \ldots, S_7)\Big|_{S_i = s_i} \begin{bmatrix} S_1 - s_1 \\ S_2 - s_2 \\ \cdot \\ \cdot \\ \cdot \\ S_7 - s_7 \end{bmatrix} \qquad (135)$$

where

$$\overline{J}(S_1, S_2, \ldots, S_7) = \begin{bmatrix} \dfrac{\partial e_1}{\partial S_1}, & \dfrac{\partial e_1}{\partial S_2}, & \ldots, & \dfrac{\partial e_1}{\partial S_7} \\[2mm] \dfrac{\partial e_2}{\partial S_1}, & \dfrac{\partial e_2}{\partial S_2}, & \ldots, & \dfrac{\partial e_2}{\partial S_7} \\[2mm] \cdot & \cdot & \cdots & \cdot \\ \cdot & \cdot & \cdots & \cdot \\ \cdot & \cdot & \cdots & \cdot \\ \dfrac{\partial e_7}{\partial S_1}, & \dfrac{\partial e_7}{\partial S_2}, & \ldots, & \dfrac{\partial e_7}{\partial S_7} \end{bmatrix} \qquad (136)$$

The elements of the Jacobian were derived analytically, and, because of the number of equations required to derive them, they will not be shown. If $J(S_1, S_2, \ldots, S_7)\Big|_{S_i=s_i}$ is nonsingular, then

$$
\begin{bmatrix} S_1 \\ S_2 \\ \cdot \\ \cdot \\ \cdot \\ S_7 \end{bmatrix} = \begin{bmatrix} s_1 \\ s_2 \\ \cdot \\ \cdot \\ \cdot \\ s_7 \end{bmatrix} - \bar{J}^{-1}(S_1, S_2, \ldots, S_7)\Big|_{S_i=s_i} \begin{bmatrix} e_1(S_1, S_2, \ldots, S_7) \\ e_2(S_1, S_2, \ldots, S_7) \\ \cdot \\ \cdot \\ \cdot \\ e_7(S_1, S_2, \ldots, S_7) \end{bmatrix} \tag{137}
$$

This equation can be rewritten as

$$
\begin{bmatrix} S_1 \\ S_2 \\ \cdot \\ \cdot \\ \cdot \\ S_7 \end{bmatrix} = \begin{bmatrix} s_1 \\ s_2 \\ \cdot \\ \cdot \\ \cdot \\ s_7 \end{bmatrix} - \frac{\bar{J}^{T}(S_1, S_2, \ldots, S_7)\Big|_{S_i=s_i}}{\det \bar{J}(S_1, S_2, \ldots, S_7)\Big|_{S_i=s_i}} \begin{bmatrix} e_1(S_1, S_2, \ldots, S_7) \\ e_2(S_1, S_2, \ldots, S_7) \\ \cdot \\ \cdot \\ \cdot \\ e_7(S_1, S_2, \ldots, S_7) \end{bmatrix} \tag{138}
$$

Therefore, from the iterative method described, one is able to obtain values of V, W, δ_a, α', β', r'_{ol}, and r'_i, which satisfy equations (123) to (129). With V, W, δ_a, α', β', r'_{ol}, and r'_i known and given equations (18) to (20) and (24), the contact loads Q_i, Q_{ol}, and Q_{or} and contact angles β_i, β_{ol}, and β_{or} can be evaluated.

DERIVATION OF FATIGUE LIFE

From the weakest link theory, on which the Weibull equation is based, we get the relation between life of an assembly (the bearing) and its components (the inner and outer rings):

$$\frac{1}{L} = \frac{12n_i}{1 \times 10^6} \left[\left(\frac{1}{L_i}\right)^{10/9} + \left(\frac{1}{L_{ol}}\right)^{10/9} + \left(\frac{1}{L_{or}}\right)^{10/9} \right]^{9/10} \tag{139}$$

In this equation life L is expressed in hours. A material improvement factor of five (to be consistent with other investigations, e.g., ref. 8) has been assumed; however, no adjustment factors for reliability or operating conditions have been added. For point contact

$$L = \left(\frac{P}{Q}\right)^3 \tag{140}$$

Therefore, equation (139) becomes

$$L = \frac{1 \times 10^6}{12n_i} \frac{1}{\left[\left(\frac{Q_i}{P_i}\right)^{10/3} + \left(\frac{Q_{ol}}{P_{ol}}\right)^{10/3} + \left(\frac{Q_{or}}{P_{or}}\right)^{10/3} \right]^{0.9}} \tag{141}$$

The contact loads are defined by equation (24). From Lundberg and Palmgren (ref. 9) the following can be written:

$$P = (2.75 \times 10^8) D^{1.8} \left(\frac{T_1}{T}\right)^{3.1} \left(\frac{\zeta}{\zeta_1}\right)^{0.4} \left(\frac{\partial \mathscr{E}}{\pi D \rho}\right)^{2.1} (k)^{0.7} \left(\frac{D}{d}\right)^{0.3} u^{-1/3} \tag{142}$$

With proper subscripting of i, ol, and or this equation can represent the dynamic load capacities of the inner ring P_i, the left outer ring P_{ol}, and the right outer ring P_{or}.

Variations of the T and ζ functions with curvature over the range from 0.52 to 0.54 are 2.3 and 0.8 percent, respectively. The variation of the product of these functions over the curvature range from 0.52 to 0.54 is less than 2 percent. Therefore, for the range just described, the products of the T and ζ functions can be considered to be constants in equation (142), or

30

$$\left(\frac{T_1}{T}\right)^{3.1} \left(\frac{\zeta}{\zeta_1}\right)^{0.4} = 0.718 \tag{143}$$

The number of stress cycles per revolution for each contact is, to a good approximation,

$$u_i = Z \left(1 - \frac{\Omega_c}{\Omega_i}\right) \tag{144}$$

$$u_o = Z \frac{\Omega_c}{\Omega_i} \tag{145}$$

Substituting equations (143) to (145) into equation (142), one can write the dynamic load capacity at the inner ring and left and right outer rings as

$$P_i = \frac{1.97 \times 10^8}{d_i^{0.3}} \left(\frac{2\mathscr{E}_i}{\pi \rho_i}\right)^{2.1} k_i^{0.7} \left[Z \left(1 - \frac{\Omega_c}{\Omega_i}\right)\right]^{-1/3} \tag{146}$$

$$P_o = \frac{1.97 \times 10^8}{d_o^{0.3}} \left(\frac{2\mathscr{E}_{ol}}{\pi \rho_{ol}}\right)^{2.1} k_{ol}^{0.7} \left[Z \left(\frac{\Omega_c}{\Omega_i}\right)\right]^{-1/3} \tag{147}$$

Therefore, from equations (24), (141), (146), and (147) the life (in hours) of the arched bearing can be obtained. The equations for a conventional bearing can be directly obtained from the arched-bearing analysis by simply letting the amount of arching be zero (g = 0) and by not considering equations related to the right outer race.

DISCUSSION OF RESULTS

A conventional 150-millimeter-ball bearing operating under pure thrust load was used for the computer evaluation. Bearing parameter and results such as life, contact loads, contact angles, spin-roll ratio, cage to shaft speed ratio, and maximum compressive stress are shown in tables I and II. The initial diametral play S_d (fig. 2) was set

fixed while varying the amount of arching; that is, for a given applied axial load and a given inner ring speed, the amount of diametral play S_d (fig. 2) was held fixed while considering different amounts of arching. In an arched bearing the free contact angle β becomes larger than that of the conventional bearing even though the diametral play is held constant. The greater the amount of arching (the larger the g), the higher the free contact angle.

The following observations can be made from the results in tables I and II:

(1) For high speed-light loads there is substantial increase in life for an arched bearing over that of a conventional bearing.

(2) An optimal amount of arching, when considering fatigue life is 0.254 millimeter (0.010 in.) for an axial applied load of 4450 newtons (1000 lb) and 0.381 millimeter (0.015 in.) for axial applied load of 22 200 newtons (5000 lb). However, these are not strong optimals.

(3) In an arched bearing there is considerably more spinning than in a conventional bearing.

(4) At shaft speed equal to 12 000 rpm the arched bearing has made contact with the outer right race.

(5) As the amount of arching is increased, the outer-race spin-roll ratio increases significantly. Therefore, for an axial applied load of 22 200 newtons (5000 lb), one might change the optimal amount of arching to 0.254 millimeter (0.010 in.).

(6) For a conventional bearing the spin-roll ratio of the inner-race contact is considerably larger than that of the outer-race contact. However, for an arched bearing the spin-roll ratios are of the same order for the various contacts.

(7) Because of the coordinate orientation, the right outer-race contact spin-roll ratio is of opposite sign from that of the left outer race.

(8) The advantage of using an arched bearing is less at high loads.

In trying to choose the best amount of arching to use, one is confronted with the following constraints:

    (a) The amount of arching must be large enough so that overlapping of the left and right outer-race contacts does not occur; that is, inequality (A) must be satisfied. For example, for the bearing considered $0 < g \leq 0.127$ millimeter (0.005 in.) did not satisfy inequality (A).

    (b) With arching greater than 0.381 millimeter (0.015 in.) there can be an order of magnitude more spinning occurring at the outer-race contacts.

Therefore, in lieu of the above, an amount of arching equal to 0.254 millimeter (0.01 in.) is the best when considering fatigue life and the amount of spinning.

Figure 14 shows the effect of speed on outer-race normal ball load Q_o, for an arched bearing and a conventional bearing. The axial applied load is fixed at 4450 newtons (1000 lb). It is seen how the arched outer race shares the load between the left

and right outer-race contact. As the speed is increased and more centrifugal force acts on the ball, it is seen in this figure that the value of the normal ball load for a conventional bearing is considerably higher than the left or right outer-race normal ball load of an arch bearing. The result of reducing the outer-race normal load from one large load to two smaller loads is life improvement for the arch bearing.

Figure 15 shows the fatigue life percent of improvement for an arched bearing over that of a conventional bearing for axial applied loads of 4450 and 22 200 newtons (1000 and 5000 lb). A comparison is also shown between the present results and those of references 4 and 5 where only the centrifugal force is considered. The ordinate E of figure 15 is defined by

$$E = \frac{L\big|_{g=0.254\ mm} - L\big|_{g=0}}{L\big|_{g=0}} \times 100 \tag{148}$$

Figure 15 shows that the fatigue life improvement over the conventional bearing is significant for the high-speed light-load condition. This increase results because the load is shared by the two outer-race contacts. Furthermore, this figure shows that there is little difference between the fatigue life analysis of this report and that of references 4 and 5.

Figure 16 shows the effect of speed on the absolute value of spin-roll ratio for an arch bearing and a conventional bearing. The applied load is held fixed at 4450 newtons (1000 lb). This figure shows that for an arched bearing the outer-race spin-roll ratio of the arched bearing is an order of magnitude larger than that of a conventional bearing. Therefore, one might speculate that there is more heat generated in an arch bearing.

SUMMARY OF RESULTS

The results indicate that for high-speed light-load applications the arched outer-race ball bearing has significant improvement in fatigue life over that of a conventional bearing. An arching of 0.254 millimeter (0.01 in.) was found to be optimal. For an arched bearing a considerable amount of spinning occurs at the outer-race contacts.

Lewis Research Center,
    National Aeronautics and Space Administration,
        Cleveland, Ohio, July 23, 1973,
            501-24.

REFERENCES

1. Brown, Paul F.: Bearings and Dampers for Advanced Jet Engines. Paper 700318, SAE, Apr. 1970.

2. Jones, A. B.: Ball Motion and Sliding Friction in Ball Bearings. J. Basic Eng., vol. 81, no. 1, Mar. 1959, pp. 1-12.

3. Harris, T. A.: An Analytical Method to Predict Skidding in Thrust-Loaded, Angular-Contact Ball Bearings. J. Lub. Tech., vol. 93, no. 1, Jan. 1971, pp. 17-24.

4. Hamrock, B. J.; and Anderson, W. J.: Analysis of an Arched Outer-Race Ball Bearing Considering Centrifugal Forces. J. Lub. Tech., vol. 95, no. 3, July 1973.

5. Hamrock, Bernard J.; and Anderson, William J.: Arched-Outer-Race Ball-Bearing Analysis Considering Centrifugal Forces. NASA TN D-6765, 1972.

6. Timoshenko, S.: Theory of Elasticity. McGraw-Hill Book Co., Inc., 1934, pp. 63-68.

7. Haines, D. J.; and Edmonds, M. J.: A New Design of Angular Contact Ball Bearing. Proc. Inst. Mech. Eng., vol. 185, 1970-1971, pp. 382-393.

8. Harris, Tedric A.: Rolling Bearing Analysis. John Wiley & Sons, Inc., 1966.

9. Lundberg, G.; and Palmgren, A.: Dynamic Capacity of Rolling Bearings. Acta Polytech., Mech. Eng. Ser., vol. 1, no. 3, issue 7, 1947.

TABLE I. - CHARACTERISTICS OF CONVENTIONAL BEARING (g = 0) UNDER APPLIED AXIAL LOAD

[Inner-raceway groove curvature, 0.54; outer-raceway groove curvature, 0.52; pitch diameter, 187.55 mm (7.3838 in.); ball diameter, 22.23 mm (0.8750 in.); diametral play, 0.2499 mm (0.0098 in.); number of balls, 22.]

| Applied axial load, F_a, N (lb) | Rotational speed of inner raceway, n_i, rpm | Life, L, hr | Raceway load, Q, N | | Raceway contact angle, β, deg | | Raceway spin-roll ratio, ω_S/ω_R | | Cage to shaft speed ratio, Ω_c/Ω_i | Raceway maximum compression stress, σ_M, N/cm^2 | |
			Inner	Outer	Inner	Outer	Inner	Outer		Inner	Outer
4 450 (1000)	12 000	12 496	419.7	1844	28.94	4.95	0.4804	0.0148	0.4693	1.013×10^9	1.302×10^9
	16 000	2 291	452.9	2995	26.60	3.08	.4625	.0148	.4672	1.040	1.5306
	20 000	583	518.5	4403	23.00	1.97	.3949	.0027	.4605	1.090	1.740
	24 000	192	708.2	5849	19.02	1.48	.3339	.0024	.4553	1.212	2.046
22 200 (5000)	12 000	806	2117	3406	29.17	14.95	0.3620	0.0575	0.4578	1.737×10^9	1.600×10^9
	16 000	378	2211	4577	27.71	10.72	.3888	.0455	.4596	1.764	1.764
	20 000	155	2435	6164	24.88	7.79	.3677	.0330	.4574	1.824	1.948
	24 000	59	2903	8226	20.58	5.86	.3109	.0295	.4522	1.937	2.144

TABLE II. - CHARACTERISTICS OF ARCH BEARING UNDER APPLIED AXIAL LOAD

[Inner raceway groove curvature, 0.54; outer raceway groove curvature, 0.52; pitch diameter, 187.55 mm (7.3838 in.); ball diameter, 32.23 mm (0.8750 in.); diametral play, 0.2499 mm (0.0098 in.); number of balls, 22.]

Applied axial load, N (lb)	Rotational speed of inner raceway, rpm	Life, hr	Raceway load, N			Raceway contact angle, deg			Raceway spin-roll ratio			Cage to shaft speed ratio, Ω_c/Ω_i	Raceway maximum compressive stress, N/cm²		
			Inner, Q_i	Left outer, Q_{ol}	Right outer, Q_{or}	Inner, β_i	Left outer, β_{ol}	Right outer, β_{or}	Inner, ω_{Si}/ω_{Ri}	Left outer, $\omega_{Sol}/\omega_{Rol}$	Right outer, $\omega_{Sor}/\omega_{Ror}$		Inner, σ_{Mi}	Left outer, σ_{Mol}	Right outer, σ_{Mor}
Amount of arching, g, 0.254 mm (0.010 in.)															
4 450 (1000)	12 000	31 602	389.8	1288	535.0	28.52	17.25	15.37	0.5806	0.3493	-0.2377	0.4639	988.7×10⁶	1158×10⁶	863.2×10⁶
	16 000	8 368	422.1	1807	1093	25.76	16.96	15.44	.4966	.3206	-.2611	.4543	1016	1296	1096
	20 000	2 440	491.4	2452	1798	21.65	16.70	15.48	.3978	.3010	-.2760	.4458	1071	1435	1293
	24 000	792	671.2	3257	2651	15.34	16.48	15.46	.2705	.2908	-.2815	.4367	1191	1577	1472
22 200 (5000)	12 000	975	2040	3111	452.8	30.21	18.93	13.39	0.5182	0.2759	-0.2037	0.4661	1717×10⁶	1554×10⁶	816.3×10⁶
	16 000	520	2112	3834	730.6	27.47	19.02	13.13	.5542	.3821	-.1988	.4606	1737	1666	957.7
	20 000	274	2320	4571	1469	23.80	18.60	13.33	.4604	.3588	-.2160	.4490	1795	1766	1209
	24 000	124	2837	5490	2557	18.63	18.07	13.59	.3314	.3192	-.2486	.4388	1924	1877	1453
Amount of arching, g, 0.381 mm (0.015 in.)															
4 450 (1000)	12 000	35 072	404.3	1174	701.0	28.65	25.27	28.65	0.5445	0.4701	-0.4585	0.4530	1000×10⁶	1125×10⁶	1000×10⁶
	16 000	7 972	447.1	1738	1280	25.94	25.03	24.43	.4836	.4636	-.4576	.4464	1036	1282	1158
	20 000	2 195	525.0	2431	1983	21.91	24.81	24.29	.3998	.4590	-.4544	.4378	1095	1434	1340
	24 000	709	719.3	3266	2827	15.77	24.59	24.13	.2803	.4545	-.4508	.4278	1218	1582	1507
22 200 (5000)	12 000	1 185	1902	2834	437.6	30.13	26.35	23.11	0.6122	0.5318	-0.3930	0.4547	1675×10⁶	1510×10⁶	809.4×10⁶
	16 000	621	2044	3432	1087	27.66	25.94	23.17	.5239	.4862	-.4281	.4476	1718	1609	1096
	20 000	277	2393	4265	2050	24.21	25.50	23.18	.4424	.4677	-.4372	.4412	1813	1730	1364
	24 000	114	2980	5335	3175	19.25	25.14	23.10	.3416	.4589	-.4366	.4322	1955	1864	1566
Amount of arching, g, 0.508 mm (0.020 in.)															
4 450 (1000)	12 000	32 838	414.8	1146	793.6	28.81	34.32	33.95	0.5466	0.6782	-0.6778	0.4330	1009×10⁶	1120×10⁶	990.8×10⁶
	16 000	7 487	450.0	1709	1357	26.14	34.05	33.73	.4879	.6717	-.6717	.4265	1038	1280	1185
	20 000	2 073	552.1	2399	2048	22.18	33.77	33.49	.4054	.6650	-.6652	.4183	1093	1433	1359
	24 000	677	700.1	3229	2878	16.18	33.48	33.23	.2881	.6581	-.6584	.4087	1207	1582	1522
22 200 (5000)	12 000	1 154	1959	2653	890.5	30.49	34.59	33.05	0.5756	0.6719	-0.6680	0.4370	1692×10⁶	1482×10⁶	1029×10⁶
	16 000	595	2105	3296	1538	28.05	34.27	32.89	.5213	.6650	-.6626	.4308	1735	1593	1235
	20 000	280	2375	4128	2381	24.58	33.92	32.68	.4474	.6575	-.6563	.4231	1808	1717	1429
	24 000	116	2916	5211	3474	19.72	33.55	32.43	.3498	.6495	-.6486	.4143	1941	1855	1620

(a) Conventional. (b) Arched.
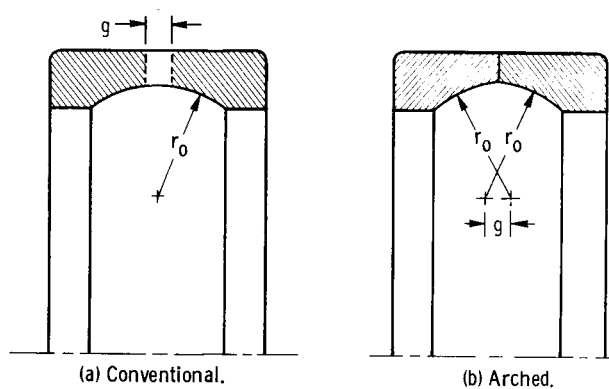
Figure 1. - Bearing outer race geometries.
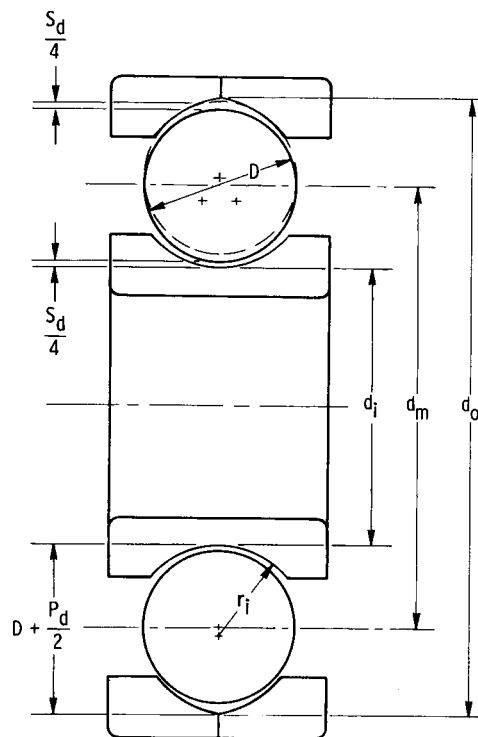
Figure 2. - Arched ball bearing in noncontacting position.

(a) Radial contact position. (b) Details of contact.
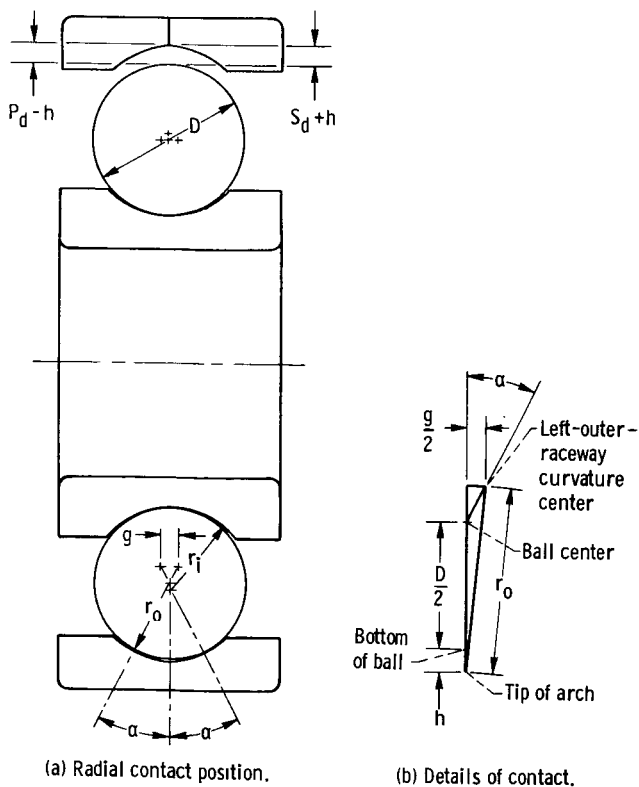
Figure 3. - Arched ball bearing radially loaded.

(b) Axial contact position of top ball. (a) Details of contact.
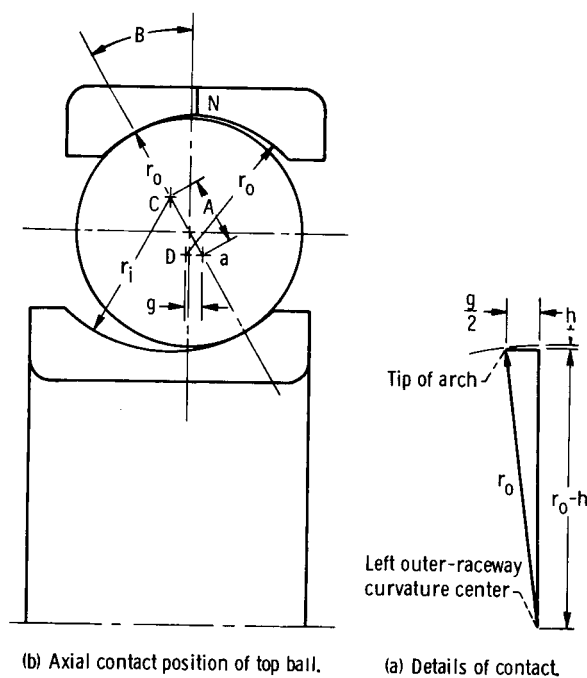
Figure 4. - Arched ball bearing axially loaded.

𝒜   Left-side outer-race curvature center
ℬ   Ball center, initial
𝒞   Inner-raceway curvature center, initial
𝒟   Right-side outer-race curvature center
𝒢   Ball center, final
𝑀   Inner-raceway groove curvature center, final
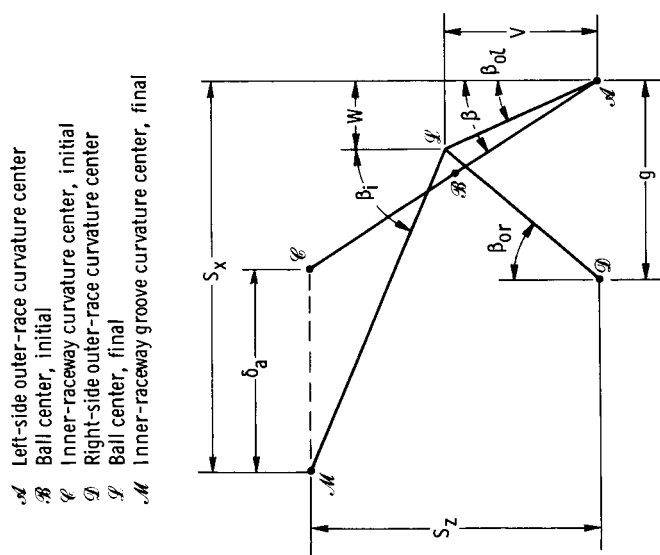
Figure 5. - Position of ball center and raceway groove curvature centers with and without centrifugal force acting on ball. Points shown for ball in top position, with bearing loaded axially.

𝒜   Left-side outer-race curvature center
ℬ   Ball center, initial
𝒞   Inner-raceway groove curvature center; initial
𝒟   Right-side outer-race curvature center
𝒮   Inner-race contact, initial
𝒦   Left-side outer-race contact, initial
𝒢   Inner-race contact, final
𝒥   Left-side outer-race contact, final
𝒦   Right-side outer-race contact, final
𝒱   Ball center, final
𝑀   Inner-raceway groove,curvature center, final

Figure 6. - Position of ball and raceway groove curvature centers and contacts with and without force acting on ball.
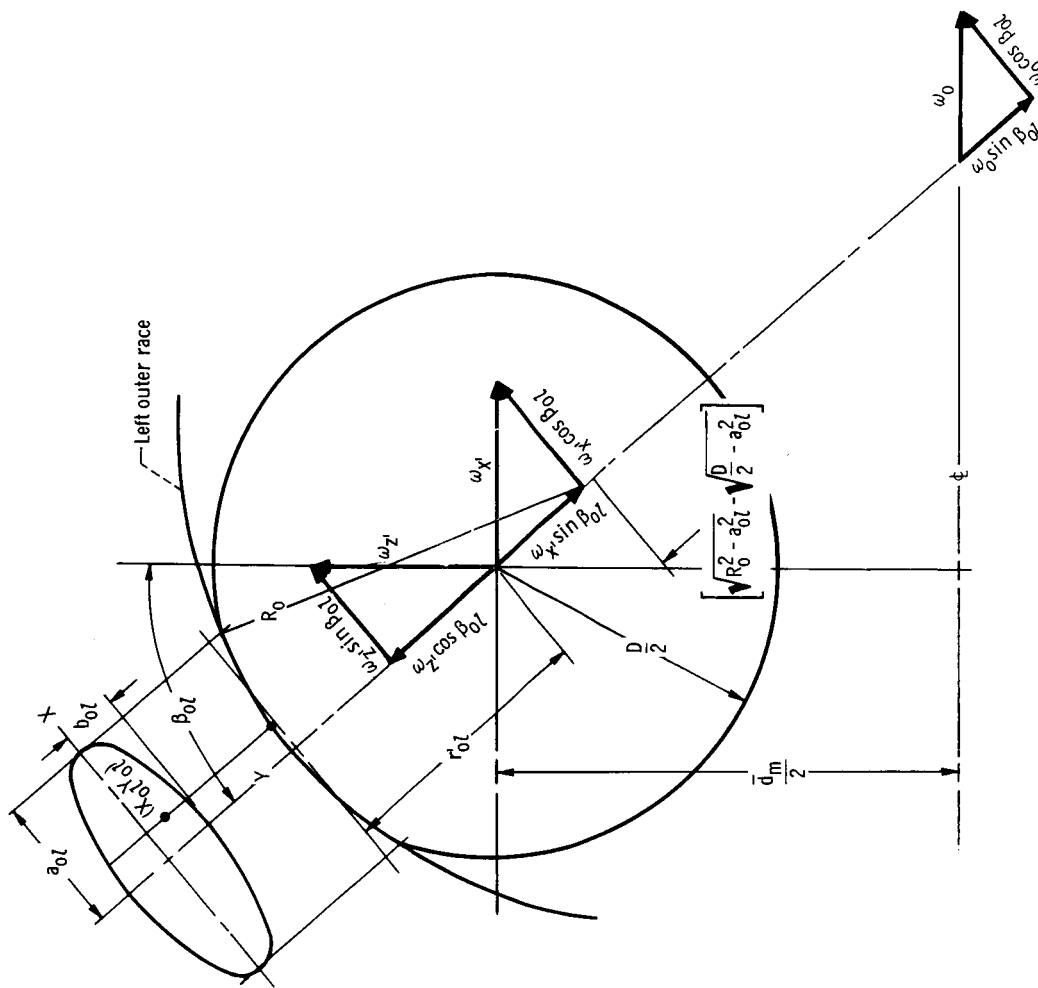
Figure 8. - Contact of ball with left outer race.
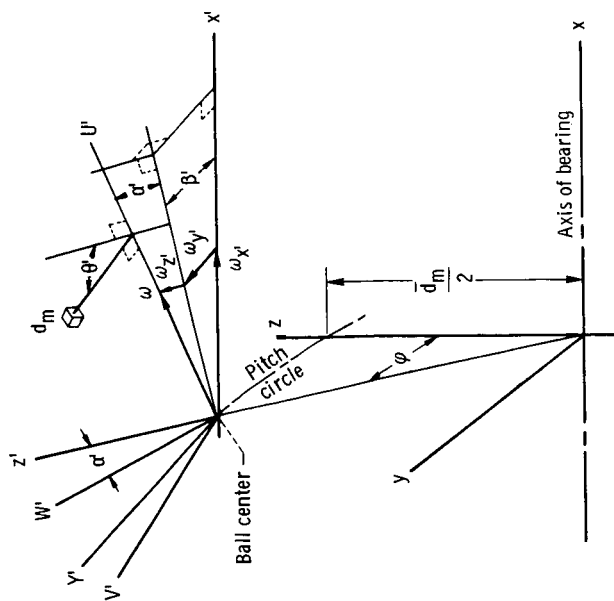
Figure 7. - Instantaneous position of element of mass in ball.

Figure 9. - Contact of ball with right outer race.
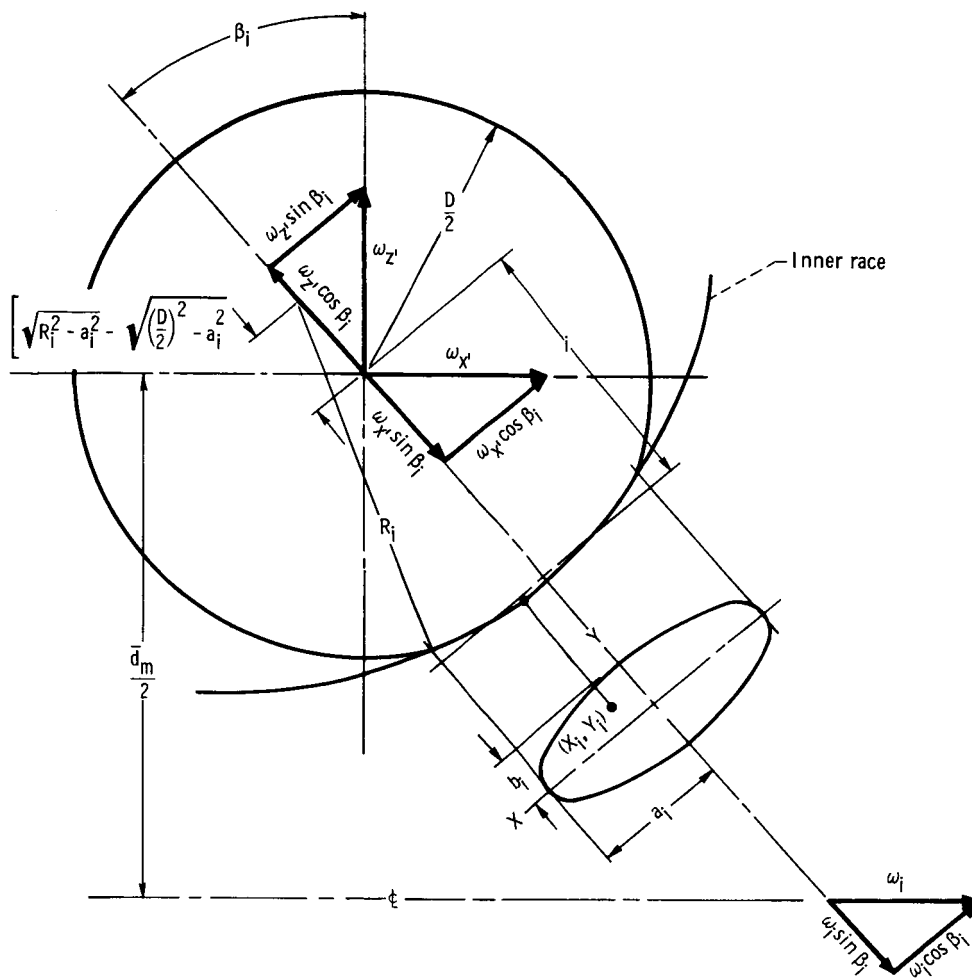
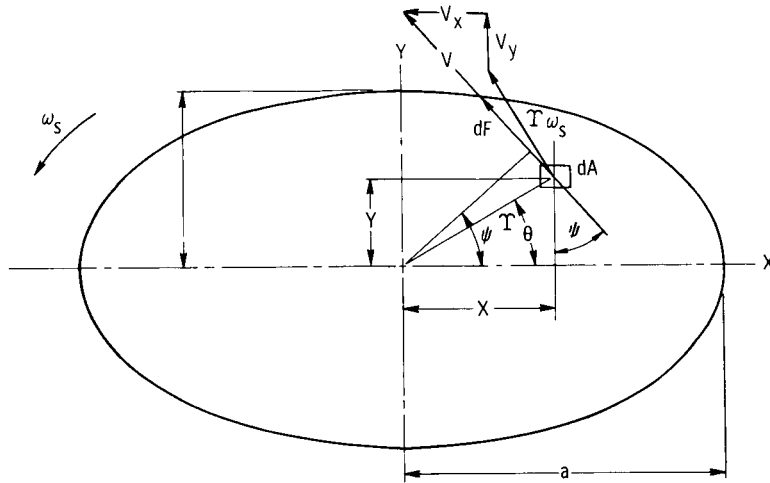Figure 10. – Contact of ball with inner race.

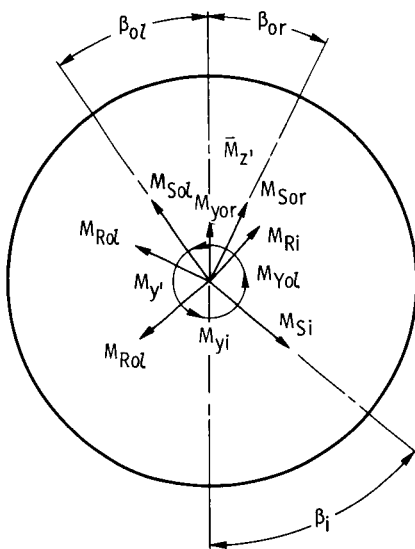Figure 11. – Enlarged view of pressure area at any of the contacts.

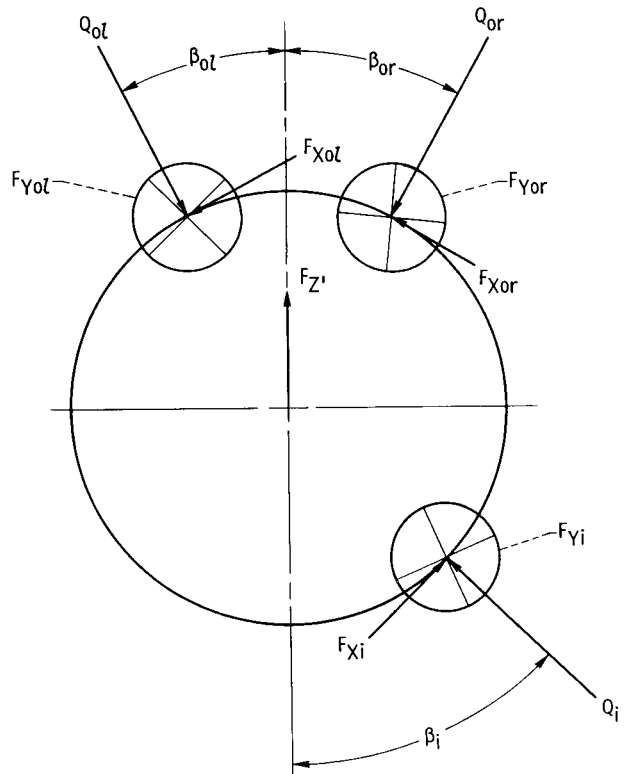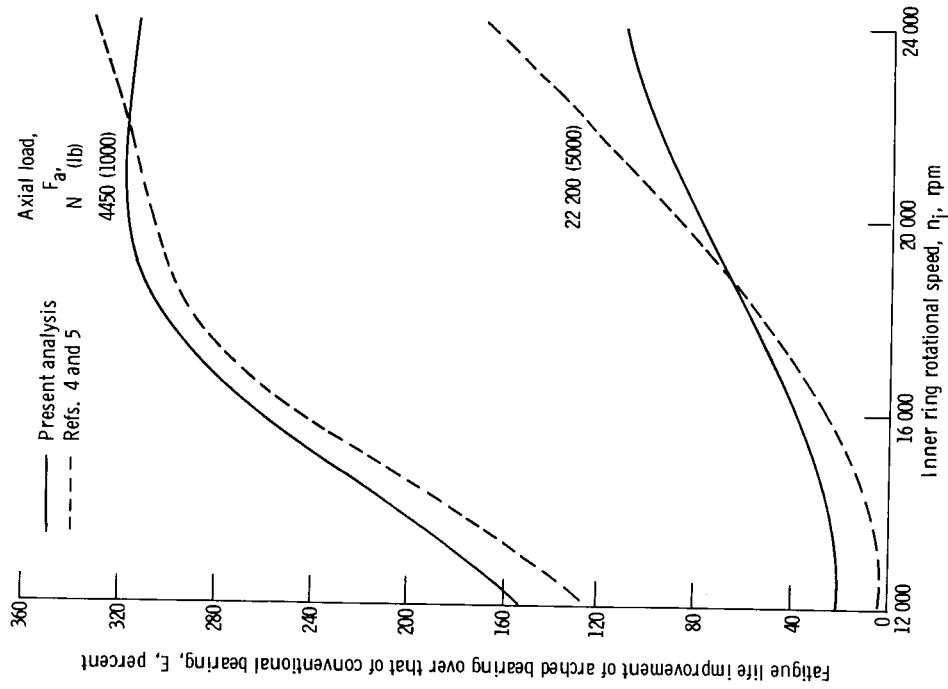Figure 12. – Moments acting on ball.

Figure 13. – Forces acting on ball.

42

Figure 15. - Effect of speed on fatigue life percent improvement of arched bearing (arching, 0.254 mm; 0.010 in.) compared with that of conventional bearing for axially applied loads of 4450 newtons (1000 lb) and 22 200 newtons (5000 lb).
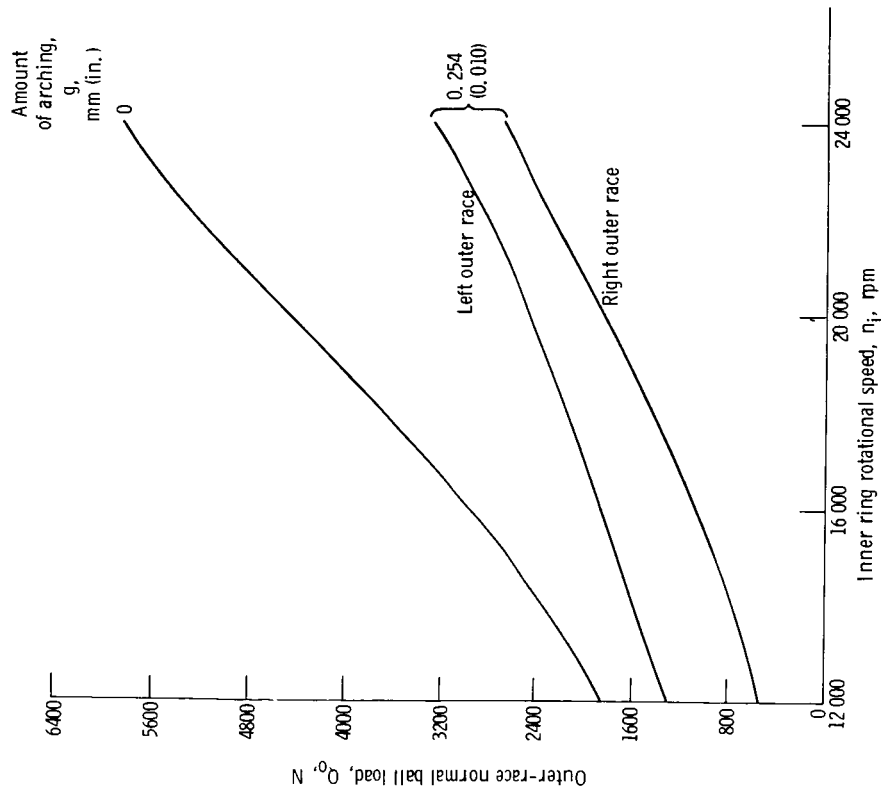

Figure 14. - Effect of speed on outer-race normal ball load, Q_o, for arched bearing (arching, 0.254 mm; 0.010 in.) and a conventional bearing (arching, 0) for axially applied load of 4450 newtons (1000 lb).
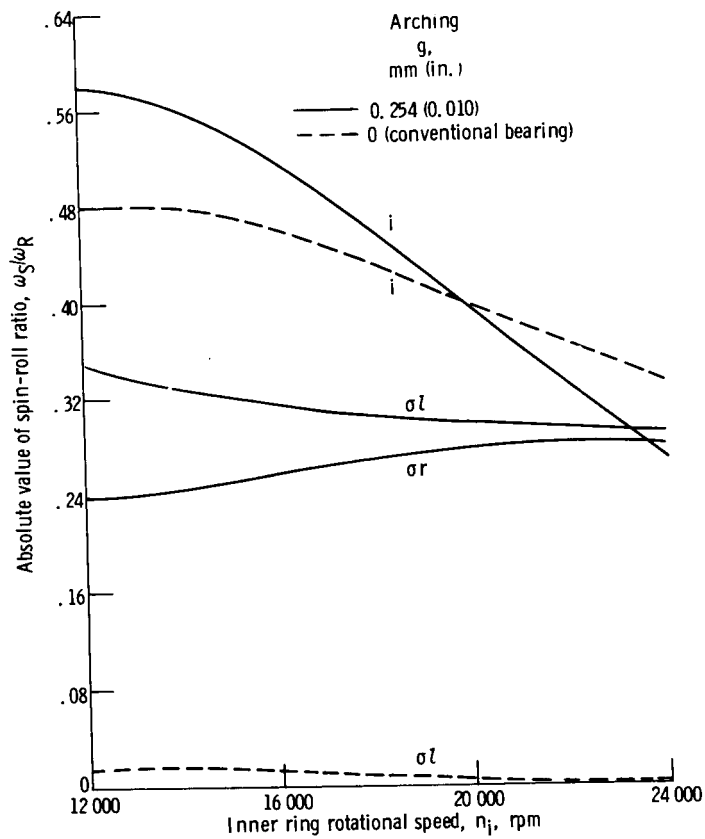
Figure 16. - Effect of speed on absolute value of spin-roll ratio for arch bearing and a conventional bearing for axially applied load of 4450 newtons (1000 lb).